Progress in PHOTOVOLTAICS

PROGRESS IN PHOTOVOLTAICS: RESEARCH AND APPLICATIONS
Prog. Photovolt: Res. Appl. 2017; **25**:67–75
Published online 11 October 2016 in Wiley Online Library (wileyonlinelibrary.com). DOI: 10.1002/pip.2814

RESEARCH ARTICLE

On the temperature dependence of dual-junction laser power converters

S. Kasimir Reichmuth*, Henning Helmers, Simon P. Philipps, Michael Schachtner, Gerald Siefer and Andreas W. Bett

Fraunhofer Institute for Solar Energy Systems ISE, Materials — Solar Cells and Technologies, Heidenhofstr. 2, 79110 Freiburg, Germany

ABSTRACT

Dual-junction GaAs laser power converters optimized for one monochromatic wavelength are presented, and their temperature dependence is experimentally evaluated. External quantum efficiency and irradiance-dependent current–voltage measurements (10 to 104 W/cm^2) under monochromatic laser light (809 nm) have been undertaken to quantify temperature- and irradiance-dependent effects on the performance. The temperature dependence of the current matching of the two subcells, caused by the temperature-dependent absorbance, is quantified. Losses in performance due to variations in operating temperature for different power-by-light applications are calculated to be between 16.2% and 21.0%. Future potential enhancements in cell performance are discussed. For elevated temperatures, super-linear behavior of the spectral response with increasing irradiance is observed, which is attributed to effective luminescent coupling from the top to the bottom subcell as the device becomes more radiative limited. For low temperatures, where the bottom cell is overproducing, no dependence on irradiance is found, which shows the influence of photon transport losses to the substrate. © 2016 The Authors. *Progress in Photovoltaics: Research and Applications* published by John Wiley & Sons Ltd.

KEYWORDS

multi-junction; power-by-light; temperature dependence; current matching; luminescence coupling; laser power converter; III–V semiconductors; photon recycling

***Correspondence**

S. Kasimir Reichmuth, Fraunhofer Institute for Solar Energy Systems ISE, Materials — Solar Cells and Technologies, Heidenhofstr. 2, 79110 Freiburg, Germany

E-mail: kasimir.reichmuth@ise.fraunhofer.de

Received 1 June 2016; Revised 1 August 2016; Accepted 17 August 2016

1. INTRODUCTION

Laser power converters are photovoltaic (PV) cells designed for the conversion of monochromatic irradiation used in optical power transmission applications. The concept of "power-by-light" is advantageous to overcome restrictions of conventional copper cabling because it inherently features galvanic isolation, avoidance of sparks, and electromagnetic interference and even enables wireless power transmission.

Application examples for this technology cover lightning safe structural health monitoring [1], high-voltage transmission line sensors [2], fuel gauges in aircrafts, smart implants [3], and rotating [4] or vacuum chamber systems. Power-by-light systems are also interesting for optical communication networks [5] and have the potential for weight reduction, for example, in aircrafts and automobiles. Typically, the necessary power for sensor applications ranges from a few milliwatts to hundreds of milliwatts. In case of actuators, the transmitted power can also range in the watt level.

Applications for laser power converters require operation under a wide range of temperatures. For example, structural health sensors in wind turbine rotor blades have to work without failure from −30 to +65 °C. High-voltage overhead lines and their galvanic isolated sensors have to perform from −20 to +75 °C [6]. In addition to the influence from ambient temperature, the actual operating temperatures of the laser power converter also depend on the system design. As opposed to the transmitter side,

where laser diodes are typically actively cooled, the PV converter at the receiver side features only passive cooling. Depending on the heat sink concept of the system, a temperature rise of the cell due to irradiation must be taken into account. In concentrating PV for comparison, cells are exposed to high irradiances and cooling is non-active as well. There, temperature dependence on irradiation has been investigated and a 4 K temperature increase per 100 W/m^2 rise in direct normal irradiance was found [7].

1.1. Photovoltaic laser power converters

Very high opto-electrical conversion efficiencies can be achieved with PV cells as power converters for monochromatic light, as the semiconductor material's bandgap can be well matched to the energy of the photons [8]. GaAs is a well-known semiconductor material that is frequently used for laser power converters. It is well matched for the 800 to 850 nm wavelength range with a bandgap of 1.42 eV at room temperature [9].

A drawback of PV cells regarding powering electronic circuitry is the low output voltage of a single cell. For a GaAs-based PV cell, the open circuit voltage is about 1 V under 0.1 W/cm^2 irradiance and increases to ~1.2 V for irradiances of 100 W/cm^2. In contrast, typical supply voltages of electronic circuitry are in the range of 3 to 12 V. However, increased voltages can be supplied by integrating appropriate power electronics, namely, DC-to-DC converters. A notable alternative solution is the series connection of several PV cells, where the total voltage equals the sum of the individual cell voltages. One way to do so is using several optical links with similar PV cells as receiver and interconnecting them in series. Another technological approach is based on monolithic integration. This can be implemented by lateral segmentation (multi-segment cell, also known as monolithic interconnected module or MIM) [10–12] or by vertical stacking of several subcells (multi-junction cell) [11–14]. In this work, cells of the latter approach are investigated, namely, vertically interconnected dual-junction cells realized by monolithic growth of two subcells on top of each other.

In a series connection, the lowest current limits the current of the entire string. For that reason, the device must be carefully designed to achieve current matching, that is, equal current generation in each subcell. For multi-junction cells, current matching is achieved by precisely tuning the thicknesses of the stacked subcells in a way that each subcell absorbs the same fraction of the incident monochromatic light [11]. Due to the Beer–Lambert law of exponential absorption in parallel with the same bandgap of each subcell, this design rule implies that the subcell thickness decreases from bottom to top (and the upmost subcell thickness decreases with increasing number of junctions) [12]. Although optimizing the subcell thicknesses in this way raises a challenge, it fits for one temperature. In real applications, the current and current matching of the device is directly affected from the temperature dependence of the absorption coefficient because the latter is directly linked to the temperature-dependent bandgap of the absorber material.

For this reason, an optimal system design which accounts for the application-dependent operating conditions requires an understanding of the impact of changing temperature on the performance of multi-junction-based PV laser power converter devices.

Therefore, in this work, the temperature dependence of dual-junction GaAs laser power converters is studied based on experimental data from cryostat measurements. The focus of this study is a quantitative understanding of the temperature-induced current mismatch of the two subcells of two different dual-junction structures.

The results are mostly applicable for monochromatic applications using dual-junction cells [11,13], yet they give insight for devices with more junctions, as recently presented in Ref. [14]. Other devices where a similar temperature dependence influences the series connection are multi-junction cells designed for the solar spectrum where "2n" junctions are realized with only "n" bandgap materials in order to boost the voltage and reduce the current [15].

2. EXPERIMENTAL

2.1. Specimen

Two dual-junction GaAs PV cell structures with different subcell thicknesses were investigated experimentally. Both structures were grown by metal organic vapor phase epitaxy. The subcell thicknesses are given in Table I. A transparent lateral conduction layer made of $Ga_{0.51}In_{0.49}P$ (1.9 eV) is included in the device on top of the top cell. The highly doped layer is a common feature of high-power laser power converters as it decreases the ohmic sheet

Table I. Overview on the investigated GaAs-based dual-junction cells.

	Top cell (GaAs)	Bottom cell (GaAs)	Measurements
Structure 1	540 nm	3.2 µm	EQE sample (T = 298…423 K)
			I–V sample (T = 150…423 K, G = 10–104 W/cm^2)
Structure 2	640 nm	3.7 µm	EQE sample (T = 273…373 K)

The structures differ in subcell thicknesses. EQE measurements were performed on both, whereas I–V measurements under laser light of varying irradiance G were solely performed on structure 1.

2017; **25**:67–75
DOI: 10.1002/pip

resistance for the lateral carrier transport from the emitter to the front contact grid fingers [16]. In between the subcells, an AlGaAs/GaAs tunnel junction is implemented to establish a low-loss series connection. Structure 2 has been described in Ref. [11].

External quantum efficiency (EQE) measurements are performed on 1 cm^2 cells with 0.4% grid shading. For high-irradiance current–voltage (I–V) measurements under laser light, a circular 0.876 mm^2 cell of structure 1 with a nominal grid shading of 6.9% is used. For the I–V measurements, a large temperature range between 150 and 423 K was chosen for detailed current mismatch evaluation. The temperature-controlled measurements were performed by using a nitrogen-cooled cryostat vacuum chamber by CryoVac [17]. Temperatures down to 100 K can be reached. The glass cover has been characterized for transmission and considered during measurements. Before loading the test samples to the cryostat, they were mounted on a planar Invar substrate to reduce mechanical stress due to different thermal expansion.

2.2. Setup

2.2.1. External quantum efficiency measurements.

A double grating monochromator setup [17] was used to measure the EQE with a spectral resolution of 10 nm. Modulated quasi-monochromatic light combined with spectrally adaptable continuous bias light is used (differential spectral responsivity method) [18]. The principle for the measurement of multi-junction devices is to bring the subcell under test into current limitation by using continuous bias light [19], which in the case of the dual-junction GaAs device requires precise filtering [11].

2.2.2. I–V measurements under monochromatic light.

In contrast to (multi-junction) solar cells, which are measured under spectrally distributed light (solar spectrum), meaningful characterization of PV laser power converters requires monochromatic light. Especially in the case of multi-junction cells with several subcells made of one absorber material, a non-monochromatic spectrum induces a strong current mismatch due to non-equivalent absorption in the subcells, which is not representative for the operation under monochromatic laser light. In the case of the investigated dual-junction GaAs structure, the use of a standard pulsed sun simulator with a Xenon flash bulb results in the bottom cell limiting the current of the complete device. Such spectrally induced current mismatch is known to lead to an overestimation of the fill factor [20] and, thus, leads to additional uncertainties for the determination of I–V parameters of these laser power converters. To overcome this limitation, a laser-based setup has been established to measure the I–V characteristics of PV laser power converters under uniform monochromatic light, in this case, 809 nm with a full width at half maximum (FWHM) of 3 nm. A schematic is shown in Figure 1 (left). In this setup, the entire I–V curve is measured within 1 ms to avoid heating of the device under test. A detailed description on this setup is published elsewhere [21]. By default, measurements are performed on a temperature-controlled chuck. For this study, it is replaced by a cryostat. In Figure 1 (right), a picture of the setup is shown.

3. RESULTS

3.1. EQE measurements

Figure 2 shows the experimental results of the temperature-dependent EQE measurements of structure 1. Top and bottom subcells are shown as solid and open symbols, respectively, while the dotted lines represent the sum of both. High-energy photons are preferentially absorbed in the thin top cell due to the high absorption coefficient at these energies. With decreasing energy, the penetration depth increases. Thus, photons are absorbed increasingly by the bottom cell. The intersections of the two subcell curves define the point of current matching. As expected from the bandgap decrease with increasing temperature [22], all curves shift toward longer wavelengths (arrows in the figure), which also holds for their intersections. Also

Figure 1. Left: Schematic of the laser setup for transient measurement of current–voltage curves for laser power converters at 809 nm. In this study, a cryostat has been added for temperature-dependent measurements over a broad temperature range. Right: Picture of the cryostat with a mounted photovoltaic cell. The black cages of the homogenizer setup are visible in the upper left corner.

DOI: 10.1002/pip

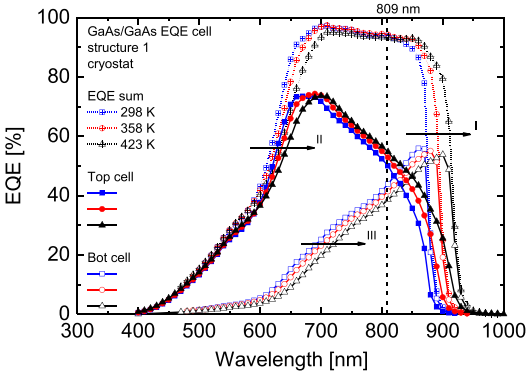

Figure 2. Temperature-dependent external quantum efficiencies of the GaAs/GaAs dual-junction device (structure 1). Top and bottom subcell curves are plotted with solid and open symbols, respectively. The dotted curves represent the sum of both subcells. All measurements were performed in 10 nm steps.

visible in the EQE graphs is the short wavelength shift, as indicated by arrow II. This is a result of the decreasing transparency due to the bandgap shift of the GaInP lateral conduction layer over temperature. The shift of the top cell towards higher wavelengths due to the shift of the bandgap influences the bottom cell correspondingly, as indicated by arrow III.

3.2. Laser I–V measurements

Current–voltage measurements under monochromatic light with a wavelength of 809 nm were carried out at various temperatures from 150 to 423 K and irradiances between 10 and 104 W/cm^2. As an example, Figure 3 shows the measured temperature-dependent I–V curves for lowest and highest measured irradiances. For other irradiances, a similar behavior is observed. At 225 K, the short-circuit current reaches a maximum. For measurements at 298 K and above, the I–V curves have high fill factors as expected (81–88%). However, at lower temperatures, a kink arises for voltages beyond the open circuit voltage which in turn leads to a decrease in fill factor. At 150 K, a second kink between maximum power point and open circuit voltage occurs.

4. DISCUSSION

4.1. EQE measurements

The behavior of the EQE data (Figure 2) is as expected and agrees well with previously reported measurements at 298 K [11]. The observed bandgap shift of −0.48 meV/K (0.3 nm/K) is in accordance with literature data for GaAs and this temperature range [23]. EQE data at 810 nm have been used to determine the temperature coefficient of the short-circuit current density TC(J_{sc}) for bottom cell limitation. It is listed in Table A1 in the Appendix to compare with the measurements at the laser I–V setup. The value is in agreement with the results of the I–V data.

The intersections of the subcell EQE curves, which correspond to the wavelength where current matching between the two subcells occurs, are extracted from the EQE measurements and plotted in Figure 4 for the two investigated structures. The plot maps the relationship among incident wavelength, cell design, and operating temperatures. For given temperature ranges, an ideal combination of laser wavelength and laser power converter can be identified. Measured data in Figure 4 are fitted linearly, with almost identical slopes. The parallel shift between the fitted curves can be understood by the main difference in design of the two devices, namely, the top cell thickness. Structure 2 has a 100 nm thicker top cell, and thus has an increased absorption compared with structure 1. This pushes the point of current matching for structure 2 toward higher wavelengths. Also shown are literature values for the bandgap of GaAs [23]. Despite the nonlinear behavior with temperature of the bandgap of GaAs, the plot shows that assumption of linear behavior is approximately valid for the investigated temperature range [22,23]. Additionally, in the plot, the temperature range for an example power-by-light application is illustrated, namely, high-voltage transmission line sensors ("high-voltage line"). Thus, temperature-dependent EQE data can serve to approximately define optimal laser wavelength and laser power converter for power-by-light systems and their operational temperature ranges. Yet, it should be noted that—opposed to the procedure of using the point of current matching as a design

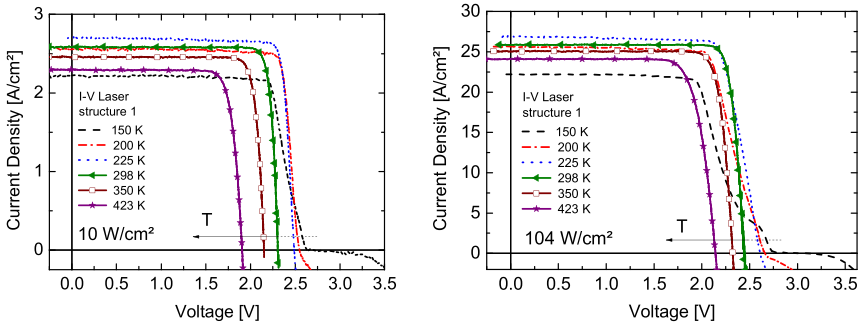

Figure 3. Current–voltage curves measured at irradiances of 10 W/cm^2 (left) and 104 W/cm^2 (right) under 809 nm monochromatic light at temperatures from 150 to 423 K.

2017; **25**:67–75
DOI: 10.1002/pip

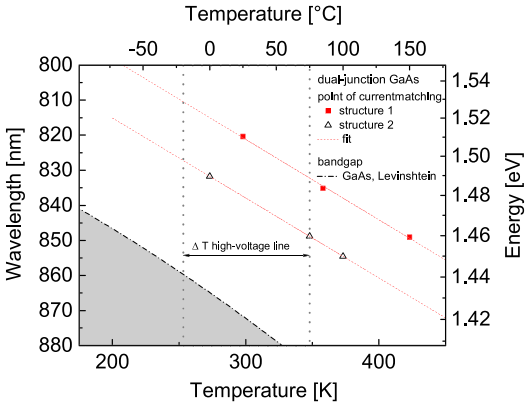

Figure 4. Plot of the temperature-dependent wavelengths at which the two subcells of the dual-junction devices are current matched. The data are extracted intersection points of the measured subcell external quantum efficiency. Dashed lines represent respective linear fits to guide the eye. For reference, the bandgap energy of GaAs is shown [23]. An example temperature range of the power-by-light application for high-voltage overhead lines is illustrated by vertical dotted lines.

criterion—thorough device optimization (with respect to temperature and wavelength) should be related to the maximum output power, that is, efficiency. Therefore, detailed I–V measurements have to be undertaken.

4.2. I–V measurements

The evaluation of the I–V measurement results is affected by a deformation of the I–V curve that occurs at low temperatures (compare dotted I–V curves in Figure 3). The observed deformation of the I–V curve occurs at a temperature of 225 K and below. Further, it becomes more pronounced with decreasing temperature as well as increasing irradiance, which a behavior is known to be originating from a majority barrier in the structure. This effect has been already observed and described in literature before [24–26]. An analogous band offset as in the reference is found in the back-surface field and the tunnel diode of the device examined in this paper. Yet, even though this effect affects the shape of the I–V curve around the open circuit voltage and also significantly influences the fill factor, the short-circuit current is not altered. Finally, for typical temperature ranges of power-by-light applications, this effect is considered irrelevant and is, thus, not discussed further.

4.3. Open circuit voltage

The measured open circuit voltage (V_{oc}) for the temperatures above 225 K is used to extract temperature coefficients TC(V_{oc}) that are listed in Table A1 in the Appendix. Lower temperatures were neglected because of the anomalous behavior described in the preceding texts. The data reveal a decreasing influence of temperature with increasing irradiance on V_{oc}. Good agreement is found in comparison with literature values of GaAs single-junction concentrator cells. At same current densities, the relative TC(V_{oc}) of structure 1 fits well into the distribution of data reported in Ref. [27]. Values of absolute TC(V_{oc}) reported in the reference range from −1.46 to −1.67 mV/K (corresponding to current densities measured at 10 W/cm^2) and −1.18 to −1.26 mV/K (current densities measured at 104 W/cm^2). For comparison of absolute values, the series connection has to be considered; therefore, half of the absolute TC(V_{oc}) for the dual-junction device is compared with the referenced values.

4.4. Short-circuit current density

Figure 5 shows the short-circuit current density J_{sc} normalized to irradiance G versus temperature for different irradiances. In this plot, the current matching between the two subcells becomes visible as a peak function. The data points are fitted linearly in order to analyze the differences in slope for both sides of the peak. For low temperatures (150–225 K), the top cell limits the full device when illuminated with 809 nm monochromatic light (compare Figure 2). Here, the slopes of the corresponding fits are almost identical and independent of irradiance. This is not the case for high temperatures (298–423 K), where the bottom cell limits the current of the device. Here, the slope—that is, the temperature sensitivity—is decreasing with increasing irradiance. As discussed in the succeeding texts, the temperature-induced current mismatch here is counterbalanced by effective luminescence coupling between the two subcells. It should be noted that the few data points around the maximum do not allow for a clear definition of the behavior, shape, and uncertainty around the point of ideal current matching. Extrapolation of the linear fits, though, indicates either an irradiance dependent

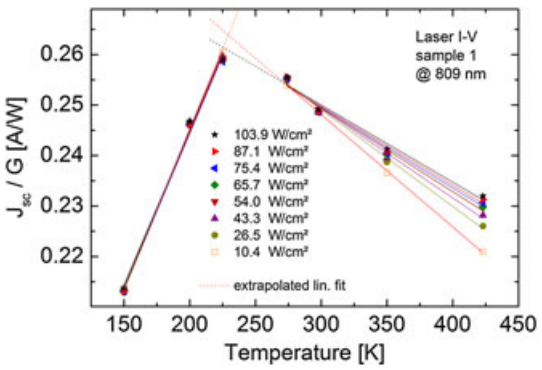

Figure 5. Plot of the short-circuit current density normalized to irradiance J_{sc}/G versus temperature. Different laser irradiances are shown as different symbols. Linear fits are applied, and extrapolations for highest and lowest irradiance are shown. For low temperatures, the top cell limits the device current, whereas for high temperatures, the bottom cell is the current limiting subcell. All data at 274 K have been measured on the Peltier-cooled chuck.

DOI: 10.1002/pip

position of the maximum or a nonlinear path of the curves close to their maximum. In the case of structure 2, we expect a very similar behavior. In Figure 4, it can be seen that current matching for the same wavelength is shifted in temperature. A similar peak is expected and shifted toward lower temperatures regarding the data of structure 1. In comparison with these two dual-junction devices, a single junction device (single segment or monolithic interconnected module) illuminated with monochromatic irradiance is expected to show almost no influence regarding temperature variations, resulting in a TC(J_{sc}) close to zero [12].

A different visualization of the same data is shown in Figure 6, where the measured short-circuit current density normalized by laser irradiance J_{sc}/G—which corresponds to the spectral response at the laser wavelength—is plotted versus irradiance for the investigated temperatures. For 150 to 298 K, the spectral response is independent of irradiance. No significant variations are noted. At higher temperatures, where the top cell is increasingly overproducing photo-generated carriers and the device becomes increasingly limited by the bottom cell, a relative gain in spectral response of 2% (350 K) and 5% (423 K) is observed when increasing the irradiance from 10 to 104 W/cm^2.

This behavior can be understood from an increasing luminescence coupling effect between the two subcells. Due to the current mismatch, the photo-generated carriers in the overproducing top cell are forced to recombine, in high-quality material to a large extent radiatively. Even though radiative recombination is a spontaneous and isotropic process, the narrow escape cone at the front surface (semiconductor/air interface) [28,29] results in an effective redirection of most of the emitted photons toward the bottom cell, where they are well absorbed due its thickness. In the end, this effect leads to an improvement in the current matching and, thus, to an increase in the current of the total device. This "self-current matching process" is super-linear with irradiance, as higher injection causes a higher internal radiative efficiency [30]. On the other hand, the gradient of the gain decreases with increasing irradiance. At high irradiance, the data in Figure 6 indicate a possible saturating behavior.

For top cell limitation (150–225 K), no nonlinear behavior is noted for the irradiance normalized current. It is expected that for greater current mismatch (i.e., lower temperatures), there is also an excess current generated in the bottom cell which will lead to an increased radiative recombination in the bottom cell as well. However, the coupling from bottom to top cell is far less efficient as from top to bottom. The isotropic emission in the bottom cell is half transmitted directly into the substrate where parasitic absorption occurs and the photons are lost. Furthermore, the photons reaching the top cell are absorbed less efficiently due to the weak absorption coefficient corresponding to emission wavelengths centered around the bandgap (see the top cell's low quantum efficiency in Figure 2), even if there is a double path due to the total internal

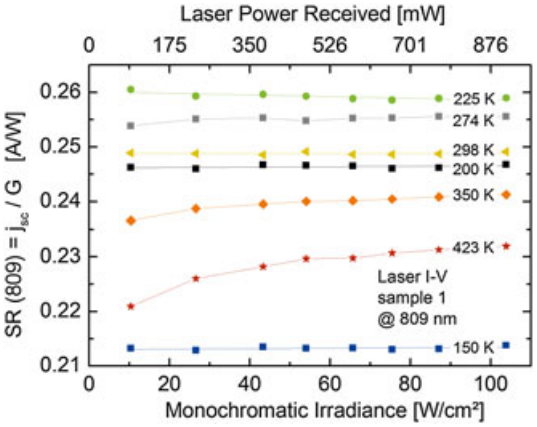

Figure 6. Short-circuit current density normalized to irradiance J_{sc}/G versus irradiance G for structure 1, measured under 809-nm laser light. The upper x-axis is calculated from irradiance, and the designated cell area $A = 0.00876\ cm^2$.

reflection from the semiconductor/air interface. An effective backside mirror at the bottom cell would add to absorption and reduce losses into the substrate.

4.5. Maximum power point

Figure 7 shows the normalized power at maximum power point (P_{mp}/G) versus temperature. It shows a similar behavior as the peak function of the normalized short-circuit current in Figure 5. It is, however, affected by the behavior of the open circuit voltage, which is decreasing with temperature and increasing with irradiance. The maximum power is further influenced by the fill factor, which is decreasing with irradiance for all measured temperatures

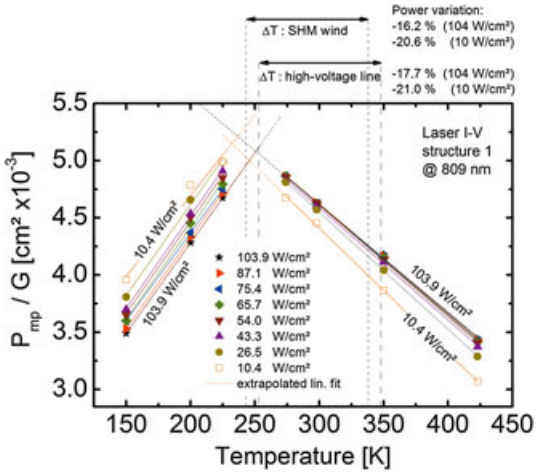

Figure 7. Power at maximum power point normalized to irradiance plotted versus temperature. Interpolated intersections are close to the lower end of the examined power-by-light temperature ranges (high-voltage line: −20… + 75 °C, structural health monitoring wind: −30… + 65 °C). Corresponding power variations for two power-by-light applications are given in the top of the plot for lowest and highest measured irradiance.

2017; **25**:67–75
DOI: 10.1002/pip

and irradiances above 26.5 W/cm^2 (Figure 3). In addition, for temperatures of 225 K and below, the aforementioned majority carrier barrier is responsible for the S-shaped kinks around V_{oc} which dramatically deteriorate the fill factor. For example, at 150 K, the fill factor drops from 80% (10.4 W/cm^2) to 68% (103.9 W/cm^2), whereas at 423 K, the fill factor only drops from 83% (10.4 W/cm^2) to 79% (103.9 W/cm^2). Due to the majority carrier barrier for lower temperatures, it leads to an inverted situation: Increasing irradiance leads to decreasing values in normalized power in the bottom cell limitation regime, whereas in the top cell limitation regime, increasing power values are reached with increasing irradiance.

In the following, we discuss output power variations due to changing operating temperatures for different power-by-light example applications. This effect is important to consider if laser power converters are used in real applications. The data shown in Figure 7 were used to quantify these output power variations according to the respective operating temperature ranges. To calculate the power variations, the maximum and minimum power value in the considered temperature interval was taken. The minimum power output is given in per cent relation to the maximum power output. Because the experimentally missing data around the peak do not allow for a clear definition of the maximum, the extrapolated fit was used to determine the maximum value. The results are shown in the top right of Figure 7.

It should also be noted that, for power-by-light systems where laser diodes are exposed to similar temperatures as the laser power converter, the performance deterioration due to temperature is expected to be softened because the laser wavelength typically shifts in a similar manner as the PV cell (e.g., 0.3 nm/K for 808-nm diode lasers). Moreover, the internal structure of a laser power converter can be optimized for the specific application. Consequently, the presented analysis can be considered a worst-case scenario but shows that temperature effects must be considered in real system applications.

5. CONCLUSION

Vertically grown dual-junction GaAs/GaAs PV laser power converters were investigated regarding their temperature and irradiance dependencies. Quantum efficiency measurements were conducted to analyze the behavior of the two subcells at three different temperatures. In particular, the point of current matching of these series-connected cells has been discussed. The relation of optimal laser wavelength to operational system temperature for two dual-junction GaAs/GaAs structures differing in top cell thickness is shown.

Extensive I–V measurements under monochromatic light of one sample have been conducted over a wide range of temperatures and irradiances. Extracted I–V parameters show the influence of temperature-dependent current matching on the performance of the device. For bottom cell current limitation, a super-linear behavior is observed due to luminescent coupling. This effect counterbalances losses due to temperature-induced current mismatch between the subcells and makes the device less sensitive to changes in operating temperatures. For top cell limitation, no significant influence from luminescent coupling is observed for the investigated irradiances and temperatures, which shows that the effective loss of photons from radiative recombination to the substrate significantly suppresses the luminescence coupling. The results obtained in this paper clearly demonstrate the necessity to characterize multi-junction laser power converters under monochromatic laser light at different irradiances, as only there the effects due to luminescence coupling between the subcells can be quantified.

Temperature coefficients of the dual-junction device are listed and show good agreement with expectations of literature values for single-junction GaAs devices. Extracted maximum power point values are used to calculate the output power variations for two different power-by-light applications and different irradiances. With increasing irradiance, the output power variations decrease.

ACKNOWLEDGEMENTS

The authors wish to thank Armin Bösch for mounting the measured samples, Martin de Boer for measurement support, Christian Karcher and Alexandre Walker for useful discussions, and David Lackner for epitaxial growth of the test structure.

REFERENCES

1. Worms K, Klamouris C, Wegh F, Meder L, Volkmer D, Philipps SP, Reichmuth SK, Helmers H, Kunadt A, Vourvoulakis J, Bett AW, Vourvoulakis J, Koos C, Freude W, Leuthold J, Stork W. Reliable and lightning-safe monitoring of wind turbine rotor blades using optically powered sensors. *Wind Energy* 2014. Published online. DOI:10.1002/we.2009.
2. Nazare FVBd, Werneck MM. Hybrid optoelectronic sensor for current and temperature monitoring in overhead transmission lines. *IEEE Sensors Journal* 2012; **12**(5): 1193–1194. DOI:10.1109/jsen.2011.2163709.
3. Park S, Borton DA, Mingyu K, Nurmikko AV, Song Y-K. An implantable neural sensing microsystem with fiber-optic data transmission and power delivery. *Sensors* 2013; **13**(5): 6014–6031. DOI:10.3390/s130506014.
4. Spillman WB Jr, Crowne DH, Woodward DW. Optically powered and interrogated rotary position sensor for aircraft engine control applications. *Optics and Lasers in Engineering* 1992; **16**(2–3): 105–118. DOI:10.1016/0143-8166(92)90003-P.

5. Röger M, Freude W, Böttger G, Dreschmann M, Huebner M, Klamouris C, Bett AW, Becker J, Leuthold J. Optically powered fiber networks. *Optics Express* 2008; **16**(26): 21821–21834.
6. Bayliss CR, Hardy BJ. *Overhead Line Conductor and Technical Specifications, in Transmission and Distribution Electrical Engineering, Chapter 18*. Elsevier Ltd, 2007. 630–692 DOI: 10.1016/B978-075066673-2/50022-7.
7. Siefer G, Bett AW. Calibration of III–V concentrator solar cells and modules. in 4th World Conference on Photovoltaic Energy Conversion. 2006. Waikoloa, USA: IEEE, DOI: 10.1109/WCPEC.2006.279563.
8. Bett AW, Dimroth F, Löckenhoff R, Oliva E, Schubert J. III–V solar cells under monochromatic illumination. in Proceedings of the 33rd IEEE Photovoltaic Specialists Conference. 2008. San Diego.
9. Höhn O, Walker AW, Bett AW, Helmers H. Optimal laser wavelength for efficient laser power converter operation over temperature. *Applied Physics Letters* 2016; **24**: 108.
10. Peña R, Algora C. The influence of monolithic series connection on the efficiency of GaAs photovoltaic converters for monochromatic illumination. *IEEE Transactions on Electron Devices* 2001; **48**(2): 196–202. DOI:10.1109/16.902716.
11. Schubert J, Oliva E, Dimroth F, Guter W, Löckenhoff R, Bett AW. High-voltage GaAs photovoltaic laser power converters. *IEEE Transactions on Electron Devices* 2009; **56**(2): 170–175.
12. Helmers H, Wagner L, Garza CE, Reichmuth SK, Oliva E, Philipps SP, Lackner D, Bett AW. Photovoltaic cells with increased voltage output for optical power supply of sensor electronics. in *SENSOR 2015 — 17th International Conference on Sensors and Measurement Technology*, Nürnberg, Germany: AMA, 2015; 519–524. DOI: 10.5162/sensor2015/D1.4.
13. Krut D, Sudharsanan R, Isshiki T, King R, Karam NH. A 53% high efficiency GaAs vertically integrated multi-junction laser power converter. in *65th Device Research Conference*, Notre Dame, IN, USA: IEEE, 2007.
14. Fafard S, York MCA, Proulx F, Valdivia CE, Wilkins MM, Arès R, Aimez V, Hinzer K, Masson DP. Ultra-high efficiencies in vertical epitaxial heterostructure architectures. *Applied Physics Letters* 2016; **108**(7): 071101. DOI:10.1063/1.4941240.
15. Moriarty T, Jablonski J, Emery K. Algorithm for building a spectrum for NREL's One-Sun multi-source simulator. *38th IEEE Photovoltaic Specialists Conference (PVSC)*, 2012; 1291–1295.
16. Oliva E, Dimroth F, Bett AW. GaAs converters for high power densities of laser illumination. *Progress in Photovoltaics: Research and Applications* 2008; **4**(16): 289–295. DOI:10.1002/pip.811.
17. Siefer G, Gandy T, Schachtner M, Wekkeli A, Bett AW. Improved grating monochromator set-up for EQE measurements of multi-junction solar cells. in *39th IEEE Photovoltaic Specialists Conference*. 2013. Tampa, FL, USA, DOI: 10.1109/pvsc.2013.6744105.
18. Metzdorf J. Calibration of solar cells. 1: the differential spectral responsivity method. *Applied Optics* 1987; **26**(9): 1701–1708.
19. Meusel M, Baur C, Létay G, Bett AW, Warta W, Fernandez E. Spectral response measurements of monolithic GaInP/Ga(In)As/Ge triple-junction solar cells: measurement artifacts and their explanation. *Progress in Photovoltaics: Research and Applications* 2003; **11**(8): 499–514. DOI:10.1002/pip.514.
20. Meusel M, Adelhelm R, Dimroth F, Bett AW, Warta W. Spectral mismatch correction and spectrometric characterization of monolithic III–V multi-junction solar cells. *Progress in Photovoltaics: Research and Applications* 2002; **10**(4): 243–255. DOI:10.1002/pip.407.
21. Reichmuth SK, Helmers H, Garza CE, Vahle D, de Boer M, Stevens L, Mundus M, Bett AW, Siefer G. Transient I–V measurement set-up for photovoltaic laser power converters under monochromatic irradiance, in *32nd European Photovoltaic Energy Conference (EU PVSEC)*, Munich, Germany, WIP, 2016; 5–10. DOI:10.4229/EUPVSEC20162016-1AO.1.2.
22. Varshni YP. Temperature dependence of the energy gap in semiconductors. *Physica* 1967; **34**(1): 149–154. DOI:10.1016/0031-8914(67)90062-6.
23. Levinshtein M, Rumyantsev S, Shur M (Eds). Si, Ge, C (Diamond), GaAs, GaP, GaSb, InAs, InP, InSb. In *Handbook Series on Semiconductor Parameters* **1**. World Scientific Publishing: Singapore, 1996. 218.
24. Hoheisel R, Bett AW. Experimental analysis of majority carrier transport processes at heterointerfaces in photovoltaic devices. *IEEE Journal of Photovoltaics* 2012; **2**(3): 398–402. DOI:10.1109/jphotov.2012.2199080.
25. Bissels GMMW, Asselbergs MAH, Bauhuis GJ, Mulder P, Haverkamp EJ, Vlieg E, Schermer JJ. Anomalous IV-characteristics of a GaAs solar cell under high irradiance. *Solar Energy Materials and Solar Cells* 2012; **104**: 97–101. DOI:10.1016/j.solmat.2012.05.001.
26. Helmers H, Schachtner M, Bett AW. Influence of temperature and irradiance on triple-junction solar subcells. *Solar Energy Materials and Solar Cells*

2013; **116**: 144–152. DOI:10.1016/j.solmat.2013.03.039.
27. Siefer G. Analyse des Leistungsverhaltens von Mehrfachsolarzellen unter realen Einsatzbedingungen, in Fachbereich Physik. 2008, Universität Konstanz: Konstanz, Germany. p. 176.
28. Schnitzer I, Caneau EY, C, Gmitter TJ. Ultrahigh spontaneous emission quantum efficiency, 99.7% internally and 72% externally, from AlGaAs/GaAs/AlGaAs double heterostructures. *Applied Physics Letters* 1993; **62**(2): 131–133. DOI:10.1063/1.109348.
29. Walker AW, Höhn O, Micha DN, Bläsi B, Bett AW, Dimroth F. Impact of photon recycling on GaAs solar cell designs. *IEEE Journal of Photovoltaics* 2015; **5**(6): 1636–1645. DOI:10.1109/jphotov.2015.2479463.
30. Walker AW, Heckelmann S, Karcher C, Höhn O, Went C, Niemeyer M, Bett AW, Lackner D. Nonradiative lifetime extraction using power-dependent relative photoluminescence of III–V semiconductor double-heterostructures. *Journal of Applied Physics* 2016; **119**(15): 155702. DOI:10.1063/1.4945772.

APPENDIX: TEMPERATURE COEFFICIENTS

The current–voltage data taken of structure 1 allow to extract temperature coefficients (TCs) for V_{oc}, J_{sc}, and P_{mp} for different laser irradiances, as shown in Table A1. For single-junction GaAs devices, the temperature dependence of the device performance is dominated by the open circuit voltage. In contrast, multi-junction GaAs cells show a significantly larger impact of the TC(J_{sc}) due to the temperature-dependent current mismatch.

Additionally, the first line in Table A1 shows TC(J_{sc}) extracted from the EQE data at 810 nm in bottom cell limitation at low irradiance in the mW/cm^2 range (precise value not known). The value fits to the results determined by the I–V measurements under laser light.

Table A1. Extracted absolute and relative temperature coefficients TC(V_{oc}, J_{sc}, and P_{mp}) as a function of monochromatic irradiance (809 nm).

Irradiance 809 nm	Laser power received cell area: 0.00876 cm^2	Abs. TC (V_{oc})	Rel. TC (V_{oc})	V_{oc} at 298 K	Abs. TC (J_{sc}) top limiting	Abs. TC (J_{sc}) bottom limiting	Rel. TC (J_{sc}) bottom limiting	Abs. TC (Pmp) top limiting	Abs. TC (Pmp) bottom limiting
[W/cm^2]	[mW]	[mV/K]	[%/K]	[V]	[mA/cm^{2}K]	[mA/cm^{2}K]	[%/K]	[mW/K]	[mW/K]
Low (EQE)							−0.097		
10.4	91.0	−3.14	−0.136	2.3055	6.59	−2.31	−0.089	0.15	−0.11
26.5	232.5	−2.81	−0.119	2.3650	16.60	−5.10	−0.077	0.42	−0.27
43.3	379.4	−2.64	−0.110	2.3931	26.94	−7.67	−0.071	0.70	−0.42
54.0	473.2	−2.58	−0.107	2.4064	33.59	−8.97	−0.067	0.87	−0.53
65.7	575.2	−2.54	−0.105	2.4172	40.41	−10.89	−0.067	1.06	−0.64
75.4	660.9	−2.51	−0.104	2.4246	46.38	−12.05	−0.064	1.16	−0.72
87.1	762.9	−2.47	−0.101	2.4339	53.75	−13.64	−0.063	1.38	−0.83
103.9	909.8	−2.42	−0.099	2.4437	63.41	−15.89	−0.061	1.64	−0.98

Values for TC(V_{oc}) are determined by using V_{oc} data from the upper three temperatures (298–423 K). Relative TC(V_{oc}) are normalized to V_{oc} at 298 K. In the first line, the relative TC(J_{sc}) for a bottom subcell limitation is given, as calculated from EQE data, where the total irradiance is in the lower mW/cm^2 range. Top cell limitation takes place for T = 150–225 K and bottom cell limitation for T = 298–423 K. All data are derived from measurements of structure 1.

DOI: 10.1002/pip